Proceedings of ASME Turbo Expo 2011
GT2011
June 6-10, 2011, Vancouver, British Columbia, Canada

GT2011-45085

CFD SIMULATIONS OF FLOW AND HEAT TRANSFER IN A PRE-SWIRL SYSTEM: INFLUENCE OF ROTATING-STATIONARY DOMAIN INTERFACE

Joachim Karnahl
Universität Stuttgart
Institute of Aerospace Thermodynamics
Pfaffenwaldring 31
70569 Stuttgart, Germany
joachim.karnahl@itlr.uni-stuttgart.de

Jens von Wolfersdorf
Universität Stuttgart
Institute of Aerospace Thermodynamics
Pfaffenwaldring 31
70569 Stuttgart, Germany
jens.vonwolfersdorf@itlr.uni-stuttgart.de

Kok-Mun Tham
Siemens Energy, Inc.
4400 Alafaya Trail
Orlando, FL 32826
USA

Mike Wilson
Department of Mechanical Engineering
University of Bath
Bath, BA2 7AY, UK

Gary Lock
Department of Mechanical Engineering
University of Bath
Bath, BA2 7AY, UK

ABSTRACT

This paper presents computational fluid dynamic (CFD) predictions of flow and heat transfer for an over-swirled low-radius pre-swirl system and comparison with experimental data. The rotor-stator CFD model comprises a stationary domain with the pre-swirl nozzles and a rotating domain with the receiver holes. The fluid-dynamic conditions feature an over-swirled system with a swirl ratio at the nozzle radius β_p = 1.4 - 1.5 and rotational Reynolds number $Re_\Phi = 0.8x10^6$ and $1.2x10^6$. Three different treatments for the rotating and stationary domain interface are used to evaluate the influence on the flow and heat transfer behavior: a stationary approach (including Coriolis forces in the rotating domain) with "direct connection" and fixed angle between pre-swirl nozzle and receiver holes; a stationary approach with circumferential averaging of the velocity at radial bands; and a full transient simulation with the rotating domain capturing the unsteady flow due to the rotating receiver holes. Results at different circumferential angles show high variability in pressure and velocity distributions at the pre-swirl inlet nozzle radius. Circumferential averaging of these flow parameters lead to an alignment of the pressures and velocities between the three different interface approaches. Comparison with experimental pressure and swirl-ratio data show a quantitative agreement but the CFD results feature a systematic overestimation outward of the pre-swirl nozzle radius. Heat transfer contours at the rotor surface show the effect of the different interface approaches and dependence on the flow structure (for example the impinging jet and vortex structures). The three different interface approaches result in significant differences in the computed heat transfer coefficients between pairs of receiver holes. Circumferentially averaged heat transfer coefficients inward of the receiver holes radius show good agreement between the transient and stationary direct connection interfaces, whereas those for the circumferential averaging interface differ, contrary to the flow parameters, due to smoothing of local effects from the pre-swirl jets.

NOMENCLATURE

a	rotor inner radius [m]
b	rotor outer radius [m]
c_p	specific heat capacity at constant pressure [J/kgK]
c_w	nondimensional mass flow rate $(= \dot{m} / \mu b)$
h	heat transfer coefficient [W/m²K]
k	thermal conductivity [W/mK]
$\dot{m}$	mass flow rate [kg/s]
p	pressure
Pr	Prandtl number $(=\mu c_p/k)$
q_w	wall heat flux [W/m²]
Q	Q-criterion [1/s²]
r	radius [m]
Re_Φ	rotational Reynolds number $(=\rho\Omega b^2/\mu)$

S	pre-swirl chamber width [m]
T	temperature [K]
u_τ	friction velocity [m/s]
v	velocity [m/s]
y^+	nondimensional wall distance ($=\rho y u_\tau/\mu$)
x,y,z	Cartesian coordinates
r,Φ,z	Cylindrical coordinates (radial, circumferential, axial)
β	swirl ratio ($=v_\Phi/\Omega r$)
θ	circumferential position
λ_T	turbulent flow parameter ($= c_w \, Re_\Phi^{-0.8}$)
μ	dynamic viscosity [kg/ms]
ρ	density [kg/m³]
Ω	angular velocity of rotor [rad/s]

Subscripts	
ad	adiabatic
atm	ambient
coarse	results of the coarser mesh
fine	results of the finer mesh
h	at receiver hole radius
i,j	indices for Cartesian coordinates
in	values at inflow boundary
max	maximum value
p	at pre-swirl nozzle radius
used mesh	results of the used mesh
w	at rotor wall
Φ	circumferential
0	total values in stationary frame

INTRODUCTION

The efficiency of gas turbines can be improved by increasing the turbine pressure ratio and the turbine inlet temperature. This requires a well balanced cooling system for the thermally-loaded components. Cooling air is diverted from the compressor (which directly reduces the efficiency of the cycle) and guided through the secondary air system to the thermally-loaded components. Part of the secondary air system supplies rotor-stator or rotor-rotor cavities where the air usually expands through pre-swirl nozzles and flows through the cavity to the receiver holes for blade cooling. Pre-swirling the air reduces the work which must be done on the flow by the rotor and consequently reduces the total temperature of the air delivered to the blades. The engine designer needs information about the pressure losses and pressure distribution as well as the heat transfer between the cooling air and turbine components. There is a diverse range of geometric configurations for the pre-swirl cavity with rotor-rotor or rotor-stator walls, with variable positions for the pre-swirl nozzles and the radius of the receiver holes.

Several experimental and numerical investigations of the performance of pre-swirl systems have been reported. One of the first experimental studies was conducted by Meierhofer and Franklin [21], presenting temperature measurements in a "direct transfer" pre-swirl system. Geis et al. [8] presented measurements of temperature and cooling efficiency in a direct transfer system. Measurements of the discharge coefficients of the pre-swirl nozzle and receiver holes were reported by Dittmann et al. [4][5][6], using the same test rig. CFD simulations of the swirl ratio, pressure losses and adiabatic effectiveness (dimensionless difference in total temperature between pre-swirl nozzle and receiver holes) of a test rig and of typical engine-representative cavity geometries were conducted by Jarzombek et al. [10][11]. Chew et al. [3] presented a numerical study and comparison with a simple drag model based on their own test rig as well as the test rig used by Dittmann et al. [4][5][6]. Lewis et al. [18] conducted a numerical study on the effect of the radial location of the pre-swirl nozzle on flow parameters and adiabatic effectiveness. Snowsill and Young [25] performed a numerical study of a high radius pre-swirl system comparing transient results with a stationary interface with circumferential averaging of the relevant flow parameters.

In addition there are several experimental, theoretical and numerical studies available, which include heat transfer to the rotating disk. Heat transfer results for a rotor-stator system with radial inflow are presented by Chen et al. [2], Djaoui et al. [7], and Pellé and Harmand [24]. An experimental and numerical study of flow and heat transfer in a direct transfer pre-swirl system was presented by Wilson et al. [26]. Karabay et al. [15][16] presented experimental and numerical results for flow and heat transfer, as well as a theoretical analysis of the adiabatic disc temperature in a rotating disc system.

The experimental data used for comparison with the calculations in this paper come from several studies at the University of Bath presented by Newton et al. [22], Yan et al. [27], Lock et al. [20][19] and Kakade et al. [13][14]. These papers describe the experimental transient measurement technique using thermochromic liquid crystals (TLC) and heat transfer measurements on the rotor of a generic low-radius pre-swirl test rig. Experiments were done at different rotational speeds and different pre-swirl flow rates, creating data over a range of rotational Reynolds numbers Re_Φ, turbulent flow parameter λ_T, and swirl ratios at the pre-swirl radius β_p. At large flow rates the measurements show a peak in the heat transfer coefficient (or Nusselt number) at the pre-swirl radius due to impingement on the rotor. At low mass flow rates, viscous effects dominate the flow field and no impingement effect was observed. Experimental data from the University of Bath test rig have been used as comparison to many CFD studies: swirl ratio, pressure distribution and heat transfer are presented by Yan et al. [27] using a 3D domain and an incompressible flow model; Lewis et al. [17] using a unstructured 3D model and CFX 5.7; Javiya et al. [12] compared different flow solvers (Hydra, Fluent, CFX) with 2D and 3D meshes, different turbulence models, with and without resolved wall treatment. These studies all showed good qualitative agreement and some reasonable quantitative agreement with the measurements but they also showed some differences especially in terms of the predicted swirl ratio.

All the above numerical studies reduced the complex two-domain problem (rotating/stationary model parts) to a one-domain problem with a circumferential slot replacing either the pre-swirl nozzles or the receiver holes. In this paper, CFD simulations are presented with a stationary and rotating domain

part to assess the effects of three different interface treatments between the rotating and stationary domains, with special interest of the capability and limitations of the interfaces to describe such rotor-stator cavity problems. The study investigates the flow and heat transfer in a pre-swirl system with a high flow rate ($1.4 < \beta_p < 1.5$) for two different rotational speeds.

EXPERIMENTAL SETUP

The experimental facility is a simplified model of a gas turbine rotor-stator system, designed to accommodate pressure and temperature instrumentation in the test section and to provide optical access to the wheel-space. Experiments were conducted at engine representative values of β_p and λ_T, thereby producing flow structures typical of those found in a gas turbine. In engines, $Re_\Phi \sim 10^7$, which is an order-of-magnitude greater than that, achievable in the rig. As heat transfer depends strongly on Re_Φ, as well as on β_p and λ_T, the test rig Nusselt numbers will be much smaller than those found in engines. CFD codes help to scale data from the test rig to the engine.

As detailed descriptions of the experimental setup and the transient thermochromic liquid crystal (TLC) measurement method are described by Lock et al. [20][19] and Kakade et al. [13][14], here only key information relevant for the numerical modelling is described.

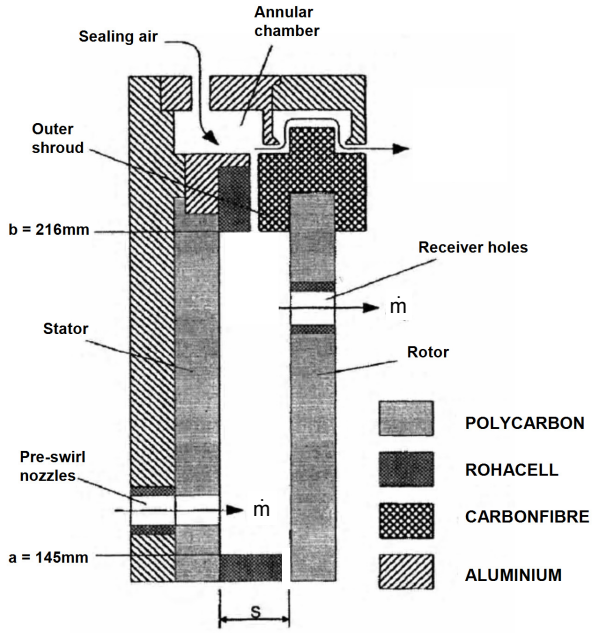

Figure 1: Schematic diagram of the rotor-stator test rig after Yan et al. [27]

Air enters the rotor-stator wheel-space (cavity) at low radius through 24 pre-swirl nozzles (cylindrical holes) which are angled 20° tangential to the stator surface. The air flows radially outward (or outboard) within the cavity and exits through 60 receiver holes on the rotating disk to ambient pressure. The gap between rotor and stator was a centred 1 mm slot at the shroud and a 1 mm slot at the hub directly at the rotor, each leading in a pressurised sealing chamber to prevent significant flows. A schematic diagram of the test rig is illustrated in Figure 1 and the geometric parameters are listed in Table 1. In the cavity the static pressures at the stator and the total pressures in the center of the cavity were measured at 10 different radial positions. The heat transfer coefficients on the rotor were determined by transient surface temperature measurements with narrow-band TLC (30°C and 40°C) and a step-change increase of the inflow temperature from an ambient value of ~ 15°C to ~ 60°C. Measurements were performed at different rotational speeds and mass flow rates. The operation range of Re_Φ, λ_T, β_p are shown in Table 1 creating a typical turbulent flow structure in the rotating cavity (Owen and Rogers [23]).

Outer disc radius b	0.216 m
Inner radius a	0.145 m
Cavity width S	0.011 m
Pre-swirl radius r_p	0.160 m
Sealing slot width	0.001 m
Receiver hole radius r_h	0.200 m
Receiver hole diameter	0.008 m
Nozzle diameter	0.0071 m
Re_Φ	0.78×10^6-1.2×10^6
λ_T	0.125-0.36
β_p	0.5-1.5
c_w	6600-27200
Rotational speed	3000-4500 rpm

Table 1: Experimental geometry and operating conditions

CFD MODEL

The 3D CFD model was built out of two rotational-symmetric domains: a stationary domain with the pre-swirl nozzles and a rotating domain with the receiver holes. Both domains are connected by an interface which is located in the cavity, parallel to the stator and rotor. The treatment of the interface is described below. The total cavity width is S = 11 mm and the total pressure measurements were located in the center of the cavity. To avoid local interface effects on the pressure at the mid-surface, the interface was located at a distance of 4 mm apart from the stator.

Mesh setup. The meshes for the two domains were generated as block-structured hexa-meshes with ICEM 12.1. The stationary mesh was built as a 15° periodic sector with one pre-swirl nozzle. The length of the pre-swirl nozzle was extended upstream to provide an orthogonal in-flow direction. The rotating mesh was built as a 6° periodic sector of the cavity using the original length of the receiver hole (i.e. that used in the experiments). However, due to backflow areas at the receiver holes exit and therefore difficulties in defining the outlet boundary condition, the receiver holes were extended.

The near-wall mesh resolution in the main cavity was modeled fine enough to resolve the boundary layer (first cell thickness = 2 µm; growth rate = 1.2). The y^+ values at the walls were usually below 1. The values of y^+ reached maximum values of 2 only around the receiver holes, the pre-swirl nozzle exit and at the in-flow location. To reduce computational effort, the receiver-hole extensions were modeled with a coarser grid

without near-wall resolution. They were also connected with an interface to the main part of the rotating domain and also in the rotating frame of reference.

Figure 2 shows exemplarily a section of the stationary mesh part. The cavity height was discretized with 204 nodes (including the O-grid nodes), the total cavity width (rotating and stationary part) with 107 nodes, the 15° sector in circumferential direction with 104 nodes and the 6° sector in circumferential direction with 42 nodes. The maximum cell length was 0.6 mm. The 15° sector mesh has ~ 1.25 million nodes, the 6° rotating sector mesh has ~0.49 million nodes and the receiver hole extension mesh has ~ 0.20 million nodes.

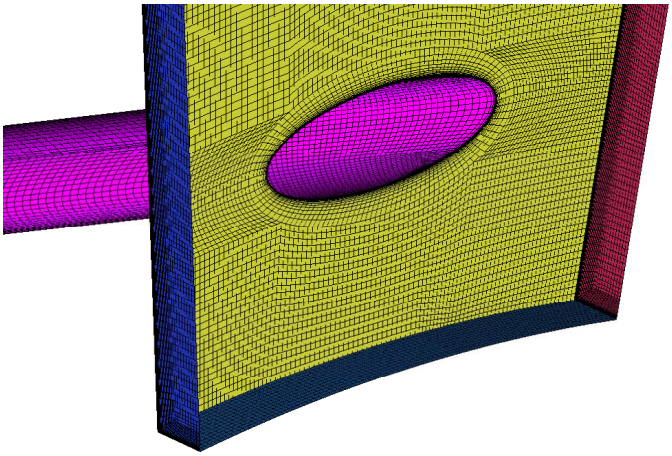

Figure 2: Section of the stationary mesh part with pre-swirl nozzle

Interface treatment. All CFD simulations were done with the commercial code CFX 12.1. The coupling between the stationary and rotating domain, where the appropriate Coriolis and centrifugal momentum terms are solved, is facilitated by interface planes which are called general grid interface (GGI). In principle there are three different options in CFX for the interface treatment. First, a full transient simulation with a rotational shift between stationary and rotating mesh at every time step (often called sliding plane), capturing the unsteady flow structures in the flow field due to the variable positions between the pre-swirl nozzle and the receiver holes. Secondly, the so called "Frozen rotor" option is a stationary approach with a "direct connection" at the interface planes without rotational offset at the interface at every time step.. This implies a fixed angle between the pre-swirl nozzle and the receiver holes. The third option is the so called "Stage" option, a stationary approach where the velocities (or pressures) are circumferentially averaged at radial bands. The Stage option has not the limitations of a "mixing plane" approach, as it can handle recirculating flow. A stationary approach saves much computational time, so one of the main questions of this study was the capability and limitations of the frozen rotor and the stage interface to describe the flow and heat transfer in a pre-swirl cavity. The GGI interface allows different pitch angles between the stationary and rotating domains; the flows, e.g. mass, momentum and energy are scaled (compressed or stretched) across the interface. This scaling leads to a systematic inaccuracy within the computational model, which increases with greater pitch ratios.

Model setup. To save computational effort most simulations for this study were conducted with a 15° stationary sector (representing one pre-swirl nozzle) and a 12° rotating domain (representing two receiver holes, i.e. a doubled 6° periodic mesh sector). Figure 3 shows the model domain, with a mesh size of ~ 2.6 million nodes. To estimate the scaling effect described above, one transient simulation with a full periodic 30° sector for both domains was computed with a mesh size of ~ 6 million nodes.

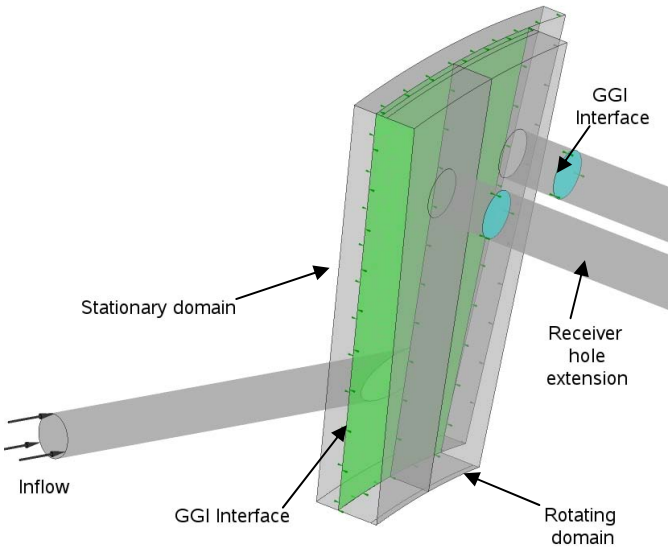

Figure 3: 15°/12° Model domain

The inflow boundary conditions for the simulations were a mass flow rate normal to the boundary surface with a turbulence intensity of 5 % and a prescribed total temperature. The outflow boundary conditions were an ambient (zero gauge) static pressure. A 1:1 mesh connection was applied at the periodic boundaries. Yan et al. [27] reported that during experiment the sealing chamber was pressurized to avoid leakage flow, but there are no measurements of the pressures in the sealing chambers reported. Therefore the two sealing slots at the inner and outer periphery were simply modeled using surfaces without wall shear. At the receiver holes extension also a free slip boundary was applied, all other walls throughout the domain were modeled with a no slip boundary. At the rotor wall heat transfer was allowed using a fixed wall temperature of 30°C (which corresponded to the TLC measurements). All other walls were assumed to be adiabatic.

The air was assumed as compressible medium using for the properties Sutherland´s law and ideal gas for viscosity and density respectively. The SST turbulence model was used, as it is the highest developed two equation eddy viscosity model implemented in CFX. The simulations were conducted with second order discretization for mass and momentum and first order turbulence discretization.

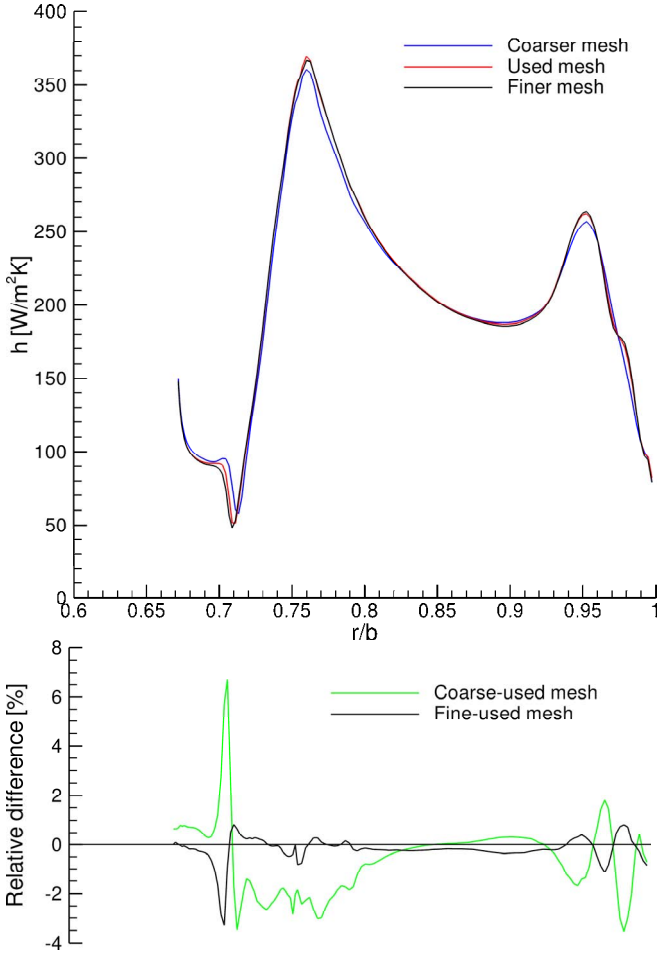

Figure 4: Mesh sensitivity: Differences in heat transfer coefficient along a radial line between receiver holes

To check the mesh sensitivity a mesh independency study was done, simulating the *"15°/12° Stage"* case also with a coarser and a finer grid. The refinement was done by a factor of 1.3-1.4 leading to a mesh size of ~ 6 million nodes. The coarsening was done by a factor of 1.4-1.6 leading to a mesh size of ~ 0.77 million nodes. Figure 4 shows the differences of the later discussed heat transfer coefficient between the three meshes along a radial line between the two receiver holes. The relative difference is calculated always in relation to the used mesh and is related to the maximum value of the used mesh:

$$\text{Relative difference} = \frac{h_{\text{coarse/fine}} - h_{\text{used mesh}}}{h_{\text{max,used mesh}}} \qquad (1)$$

It can be seen that the differences between the used mesh and the fine mesh are usually below 0.8 % except around the regions r/b ~ 0.7 and r/b > 0.95. The bigger differences at these regions result mainly from the steep curve progression and a small radial shift of the curves. The comparison between pressure and velocity distributions shows a similar behavior hence the grid resolution of the used mesh is claimed to be fine enough.

Simulation cases. The influence of the interface treatment was studied at two operation points with an over-swirled system: The first operation point was at a rotational speed of 3000 rpm with a corresponding rotational Reynolds number $Re_\Phi \approx 0.8x10^6$, a dimensionless mass flow rate c_w = 19200 and a swirl ratio at the nozzle β_p = 1.49. The second operation point was at a rotational speed of 4500 rpm ($Re_\Phi \approx 1.2x10^6$) with c_w = 27200 and β_p = 1.41. For both simulations the turbulent flow parameter was equal at λ_T = 0.37. All simulations were done with a wall temperature T_w = 30°C. Table 2 shows an overview of the simulations in this study, the labeling describes the model domain used (15°/12° sector or full periodic 30°/30° sector) the used interface type and for transient simulation if a snapshot at the last time step is used (Trans.), or the transient averaged values (Trans. ave.).

Labeling	Interface type	Comment
15°/12° Frozen rotor	Frozen rotor	
15°/12° Stage	Stage	
15°/12° Trans. ave.	Transient	transient averaged values
15°/12° Trans.	Transient	snap shot at last time step
30°/30° Trans. ave.	Transient	transient averaged values
30°/30° Trans.	Transient	snap shot at last time step

Table 2: Simulation overview

The time steps for the Frozen rotor and stage simulation were $1.5x10^{-5}$ s ($Re_\Phi = 0.8x10^6$) and $2.5x10^{-5}$ s ($Re_\Phi = 1.2x10^6$) leading to a root mean square error RMS of < $1x10^{-6}$ for the Frozen rotor simulation and a RMS < $2x10^{-5}$ for the Stage simulation. The time step of the transient simulation was ~$9.26x10^{-6}$ s representing a 0.25° rotation per time step leading to a RMS < $5x10^{-6}$. The global imbalance of all equations was below 0.5 %.

FLUID DYNAMICS

Flow structure. The typical flow in a rotor-stator cavity is driven by the rotor which accelerates the flow in radial and circumferential direction leading to a swirled core region in the cavity and a recirculation flow at the stator. In a low radius pre-swirl chamber this "cavity flow" interacts with the pre-swirl jet which enters the cavity and impinges at the rotor. Due to the rotor speed and the location of the receiver holes at a higher radius the pre-swirl nozzle jet flow is then also accelerated in radial direction. In most of our cases the flow is scaled in circumferential direction at the interface between the 15° sector and the 12° sector.

Figure 5 shows the flow velocities and streamlines on a meridional plane at pre-swirl nozzle radius r/b = 0.74 with the jet inflow from the left side in the middle. Figure 5a+d) shows the circumferential averaging of the velocities at the Stage interface as the higher jet velocities are smoothed. Also it can be seen that the streamlines in the rotational grid part which start at the interface have all the same angle due to the averaging. The scaling effect at the interface can be seen in Figure 5 b/c) with the "scaling fix point" in the upper corner between stationary and rotating domain. Plotting the stream lines in the rotating frame of reference the frozen rotor and transient interfaces show partly streamlines perpendicular to the

interface in the rotating domain part. Due to the fixed angular position between pre-swirl nozzle and receiver holes the frozen rotor interface (Figure 5e) shows a stronger impingement on the rotor than with the transient interface (Figure 5f). This leads to a higher heat transfer at this radial position which can be seen later in Figure 13a).

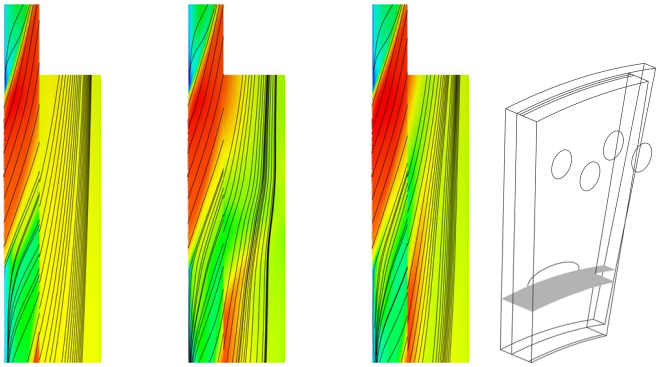

a) Stage b) Frozen rotor c) Transient
Stationary frame of reference for both domains

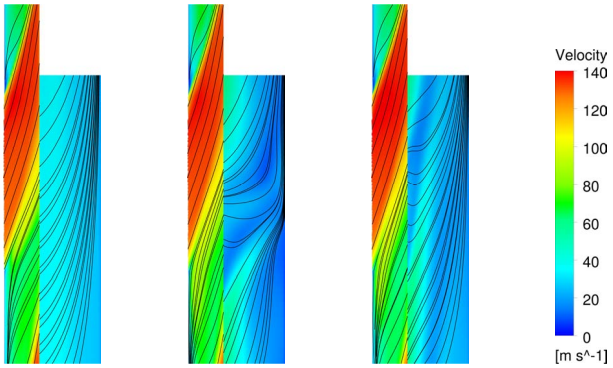

d) Stage e) Frozen rotor f) Transient
Relative frame of reference for rotating domain

Figure 5: Velocity and stream lines for the 15°/12° model on a meridional plane at pre-swirl nozzle radius r/b = 0.74 (left side = stationary domain)

Pressure. The experimental measurements of pressure at different radii were made dimensionless with respect to the pressure p_p at the pre-swirl radius r_p. Previous numerical works used usually a circumferential slot as inlet so the circumferential gauging position of p_p was less important. The numerical simulations including the pre-swirl nozzle showed that p_p is varying significantly with circumferential direction at the chosen radial position. Thus the circumferential gauging position of the pressure measurements in relation to the pre-swirl nozzle exit is significant but not reported. Therefore only the curve progression should be compared.

To show the variability of the pressure values, exemplarily the static pressure values (relative to ambient pressure) for the *"15°/12° Trans."* case with $Re_\Phi = 1.2x10^6$ are evaluated at several radial lines at different circumferential positions θ (1° steps without lines cutting the nozzle). The static pressure values are plotted against the dimensionless radius r/b in Figure 6a) and show the high variability of the pressure levels at pre-swirl nozzle radius (r/b=0.74), whereas the pressure at radii r/b > 0.82 converge.

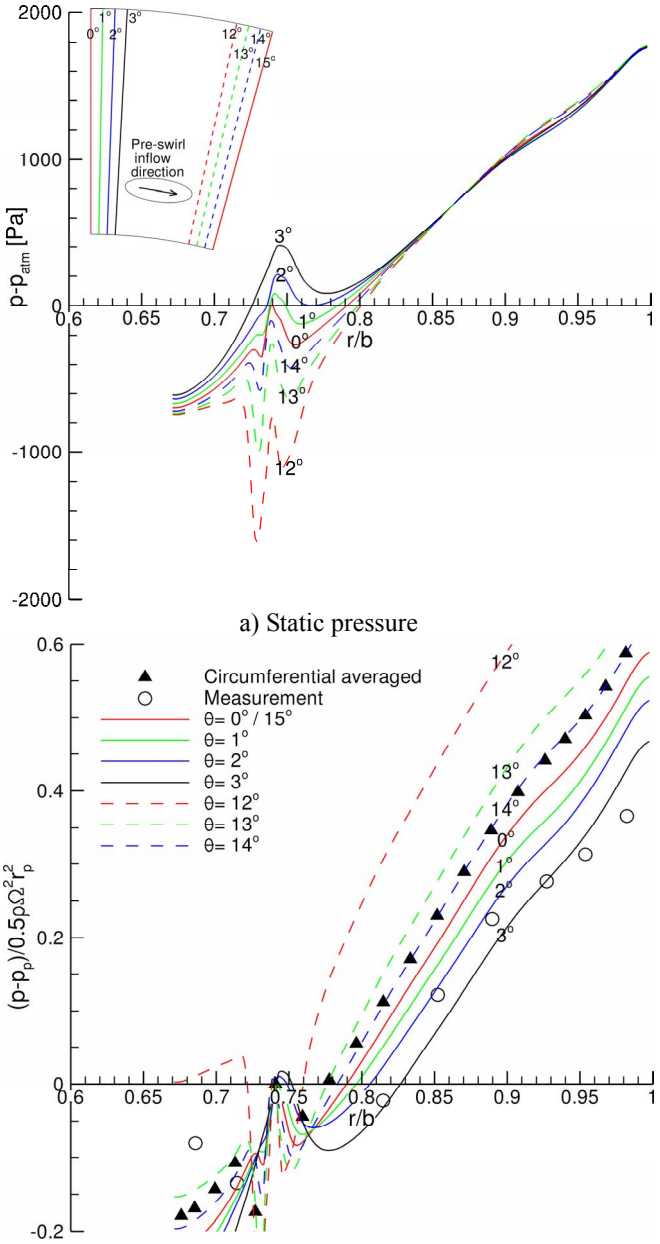

a) Static pressure

b) Dimensionless static pressure

Figure 6: Static pressure levels"15°/12° Trans.", ($Re_\Phi = 1.2x10^6$, radial lines at several positions θ)

The corresponding dimensionless pressures including the circumferentially averaged dimensionless pressure and the measurement data in Figure 6b) show that this variability of pre-swirl pressure leads to a spreading of the dimensionless pressures at radii greater than the pre-swirl nozzle radius. Additionally the numerical results show only for the lowest dimensionless pressure values a fairly good agreement with the measurement data, hence the dimensionless circumferentially averaged values show a systematic overestimation of dimensionless pressure level, but show a good agreement of the

curve progression. A similar pressure variation at pre-swirl radius can be found for the total pressure levels at the mid-surface. For further comparison of the different interface treatments only the circumferentially averaged pressure levels are used.

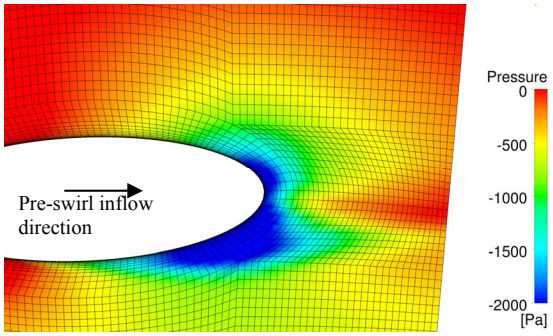

a) Static pressure at stator

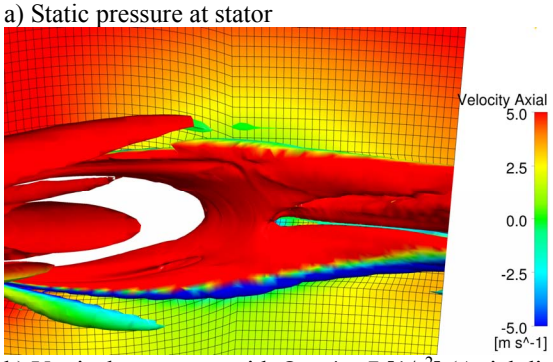

b) Vortical structures with Q = 4e+7 [1/s^2] (Axial direction exiting the image plane)

Figure 7: Detail view of pre-swirl nozzle exit

The jagged nature of the pressure behind the pre-swirl nozzle exit at r/b = 0.74 resulting from the interaction between the pre-swirl jet and the swirled core flow leading to two vortical structures in circumferential direction after the pre-swirl nozzle which influence the pressure distribution at the stator. The vorticity in the flow can be displayed by defining the Q-criterion as described by Hunt et al. [9], where with positive values of Q vorticity is more predominant than shear strain and large values of Q represent a stronger vortex:

$$Q = \frac{1}{2}\left(\frac{\partial v_i}{\partial x_j} - \frac{\partial v_j}{\partial x_i}\right)^2 - \frac{1}{2}\left(\frac{\partial v_i}{\partial x_j} + \frac{\partial v_j}{\partial x_i}\right)^2 \qquad (2)$$

The pressure distribution and the vortical structures (colored with the axial velocity) at the pre-swirl nozzle exit are shown in Figure 7.

Figure 8 shows the circumferentially averaged static pressure at the stator for the different interface treatments ($Re_\Phi = 1.2x10^6$). The averaging was done at the same radial position than in Figure 6b). The values of the static pressure show in principle the same curve progression between the different interface treatments. There is higher variability around the pre-swirl nozzle radius r/b= 0.74 with a maximum pressure difference $\Delta p \approx 288$ Pa between the Stage simulation and the Frozen rotor interface. The values of static pressure converge near the outer radius, e.g. at the receiver hole radius the differences in pressure are around $\Delta p \approx 20$ Pa, which is also an inevitable consequence of the fixed outlet pressure boundary condition at the receiver holes.

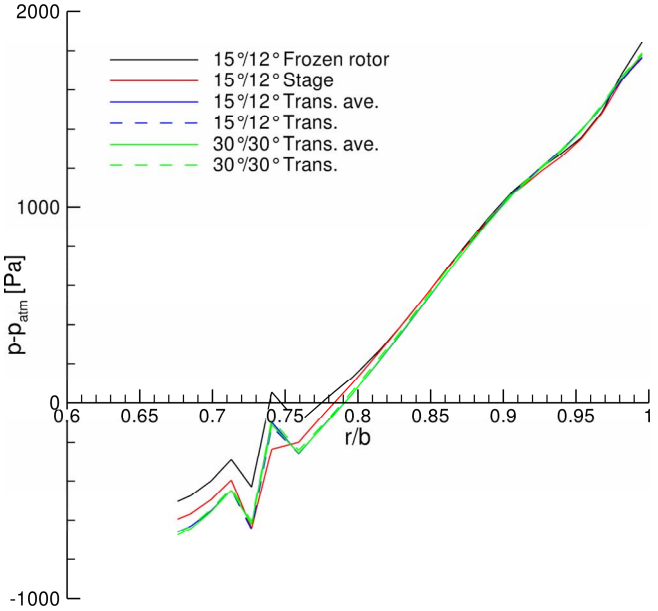

Figure 8: Circumferentially averaged static pressures at stator ($Re_\Phi = 1.2x10^6$)

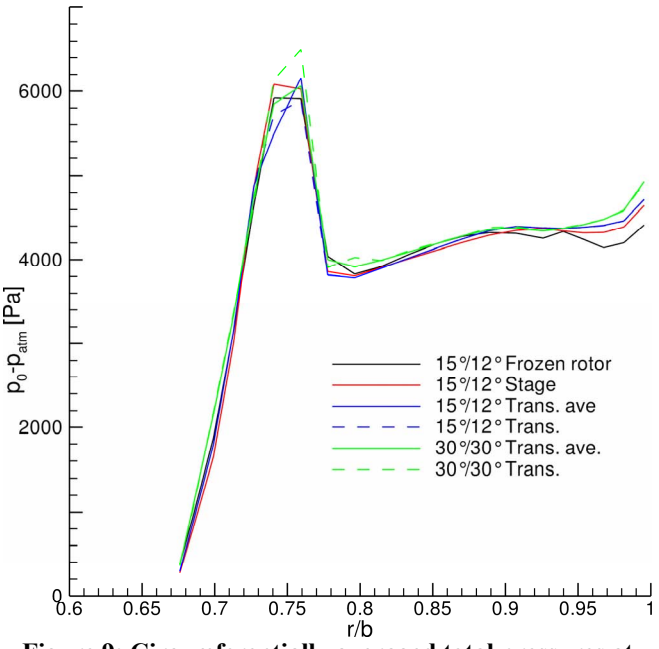

Figure 9: Circumferentially averaged total pressures at mid-surface ($Re_\Phi = 1.2x10^6$)

Figure 9 shows similar behavior for the circumferential averaged total pressure distribution at the mid-surface. The maximum pressure difference between the different interfaces of $\Delta p_0 \approx 590$ Pa is at the pre-swirl nozzle exit. These pressure results also converge with increasing radius: at the receiver

holes radius a total pressure difference of $\Delta p_0 \approx 124$ Pa is observed.

Comparing the transient averaged pressure results between the simplified 15°/12° sector model and the full 30°/30° sector model is can be seen that there is nearly no difference for the static pressure at the stator. The total pressure at the mid-surface between the simplified and the full model show a bigger difference around the pre-swirl nozzle radius indicating that the simplified model has some inaccuracy due to the scaling at the interface.

The simulations show that the circumferentially averaged static and total pressure levels in the cavity are affected by the pre-swirl jet and therefore show some deviation with different interface simulations. This influence decreases with increasing radius outward of the pre-swirl nozzle. Simulations with $Re_\Phi = 0.8x10^6$ show the same behavior and are therefore not presented here.

Swirl ratio. The dimensionless swirl ratio β at the mid-surface is shown in Figure 10 using the circumferentially averaged numerical values of v_Φ to determine β. The corresponding experimental values for v_Φ were estimated from the pressure measurements at stator and mid-surface (local values) and are shown for the later discussion of the influence of v_Φ on the heat transfer coefficient. For the circumferentially averaged values there are only small differences in the results for the different interface treatments. The different interface simulations show bigger differences in swirl ratio only in the region of the pre-swirl nozzle, outward of the pre-swirl nozzle the swirl ratio results for the different simulations agree well.

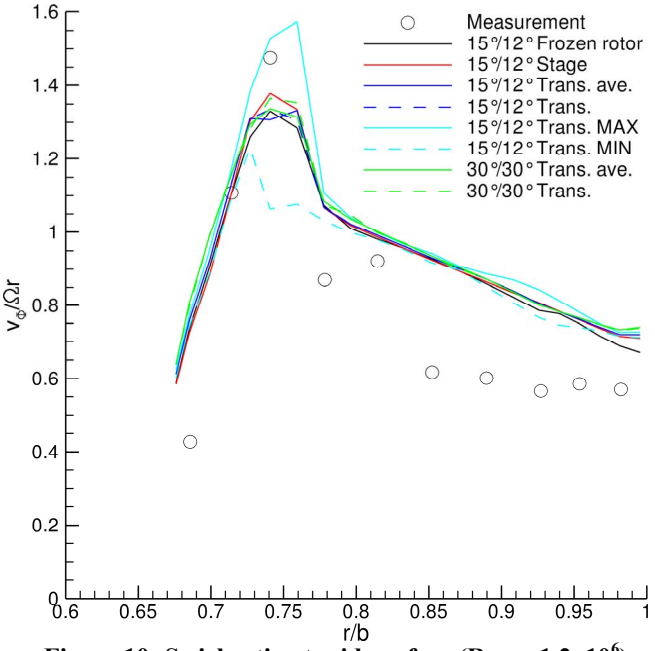

Figure 10: Swirl ratio at mid-surface ($Re_\Phi = 1.2x10^6$)

As it is important for later discussion of the heat transfer the maximum and minimum swirl ratios for the *"15°/12° Trans."* evaluation are also plotted in the diagram using maximum and minimum values from the circumferential variation of v_Φ. The maximum local swirl ratio of 1.6 is reached at r/b = 0.76 resulting from a slight deflection of the pre-swirl jet outward of the pre-swirl radius. The minimum and maximum swirl ratios for the different simulations with the Frozen rotor and transient interface differ from the circumferentially averaged values about ± 25 % at the pre-swirl radius and also converge outward of the pre-swirl nozzle radius. The stage interface does not show this difference as the circumferential averaging is carried out at the interface.

HEAT TRANSFER

To determine the heat transfer coefficients h at the rotor from numerical simulations the fixed wall temperature T_w (used as a boundary condition) and the wall heat flux q_w are taken directly from the numerical simulations:

$$h = \frac{q_w}{T_w - T_{w,ad}} \qquad (3)$$

The adiabatic wall temperature $T_{w,ad}$ is based on a theoretical adiabatic disc temperature derived by Karabay et al. [16] which was also used for experimental evaluation of the heat transfer coefficients for the experiment as:

$$T_{w,ad} = T_{0,in} - \frac{v_\Phi^2}{2c_p} + Pr^{1/3}\frac{\Omega^2 r^2}{2c_p}\left(1 - \frac{v_\Phi}{\Omega r}\right)^2 \qquad (4)$$

Here $T_{0,in}$ is the total temperature at the pre-swirl inflow boundary. With Equation 3 and 4 the influence of v_Φ on the adiabatic wall temperature calculation and the heat transfer coefficient can be quantified. In Figure 10 the maximum difference between measured and circumferentially averaged swirl ratio β (respectively v_Φ) is ~0.32 at r/b= 0.85 for the "*30°/30° Trans. ave.*" case. This difference in the swirl ratio leads to a difference of $\Delta T_{w,ad} = 2.3$ K, which is compared to the step-change increase of the inflow temperature during experiment from an ambient value of ~15°C to ~60°C quite small. The relative difference in the heat transfer coefficient resulting from $\Delta T_{w,ad}$ is 8.9 %.

Heat transfer contours. The influence of the different interfaces on the heat transfer coefficient contours can be seen in the contour plots in Figure 11. For the contour plots the heat transfer coefficient and $T_{w,ad}$ are calculated with v_Φ at each nodal position at the rotor.

As expected the highest heat transfer coefficients occur at the pre-swirl nozzle radius where there is the greatest impact of the pre-swirl flow on the rotor. The stage and transient averaged simulations show circumferentially banded heat transfer coefficient distributions at radii inward (or inboard) of the receiver hole radius, whereby the transient averaged contour plot shows higher values. The frozen rotor interface Figure 11b) shows a separate streak of high heat transfer outward of the pre-swirl nozzle radius, which occurs due to the fixed angular position between pre-swirl nozzle and receiver holes with this interface approach. The snapshots of the

transient simulation at the last time step in Figure 11d+e) show the instantaneous heat impact of the hot pre-swirl jet flow.

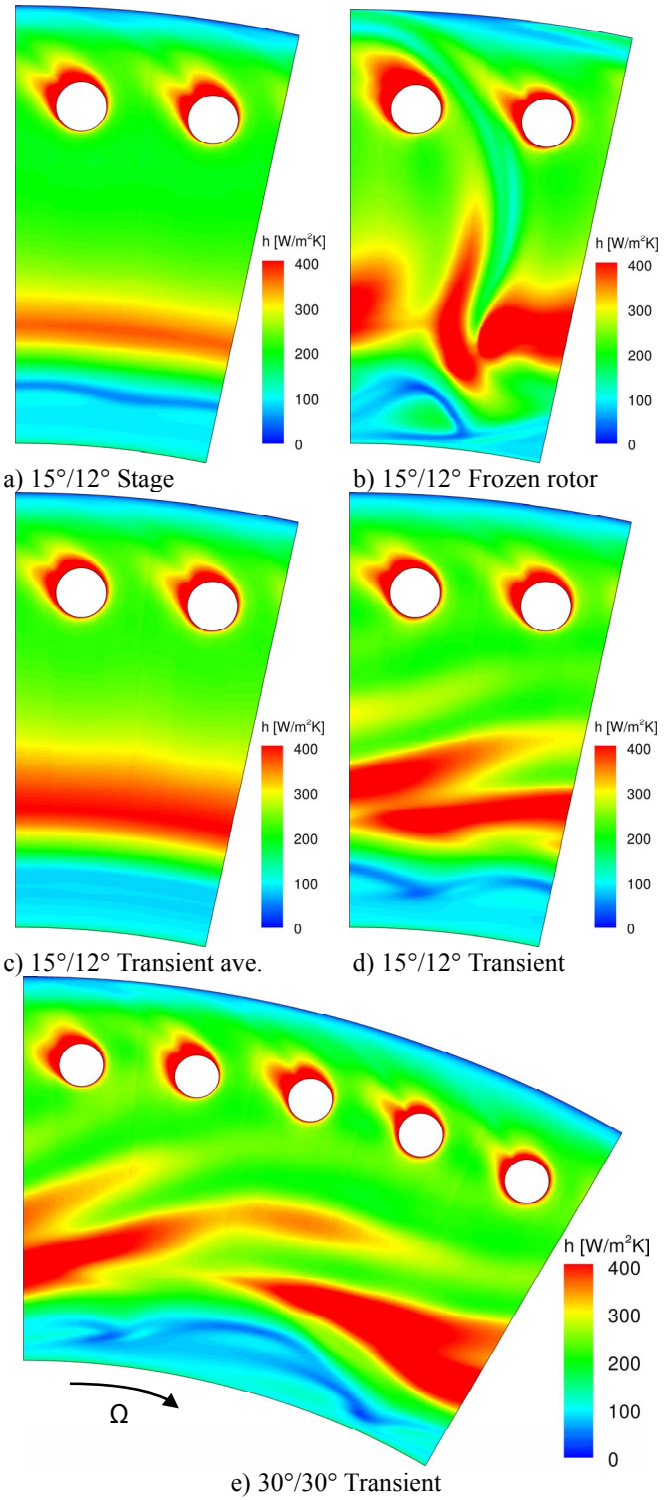

a) 15°/12° Stage
b) 15°/12° Frozen rotor
c) 15°/12° Transient ave.
d) 15°/12° Transient
e) 30°/30° Transient

Figure 11: Heat transfer contour plot (rotor) ($Re_\Phi = 1.2x10^6$)

Comparing the contour plots of the 15°/12° sector at the last time step and the full 30° sector at the last time step, it is remarkable that the full 30° sector contains two pre-swirl nozzles but does not show two periodic high heat transfer zones at the pre-swirl nozzle radius. This can be explained by a more detailed view of the turbulent pre-swirl jet flow behavior and the effect on the heat transfer. The rotor induced flow in the boundary layer can also have an effect on heat transfer, but this is not discussed here. One pre-swirl jet related mechanism for heat transfer at the rotor is impingement of the pre-swirl jet on the rotor inducing a zone of higher heat flux/heat transfer. Another mechanism is that in the circumferential direction behind the pre-swirl nozzle jet the previous mentioned two vortical structures occurs (for details see Figure 7b). These vortical structures extend in the circumferential direction. When these zones reach the next pre-swirl nozzle they are deflected to the rotor by the next pre-swirl jet inflow also inducing higher heat transfer zones.

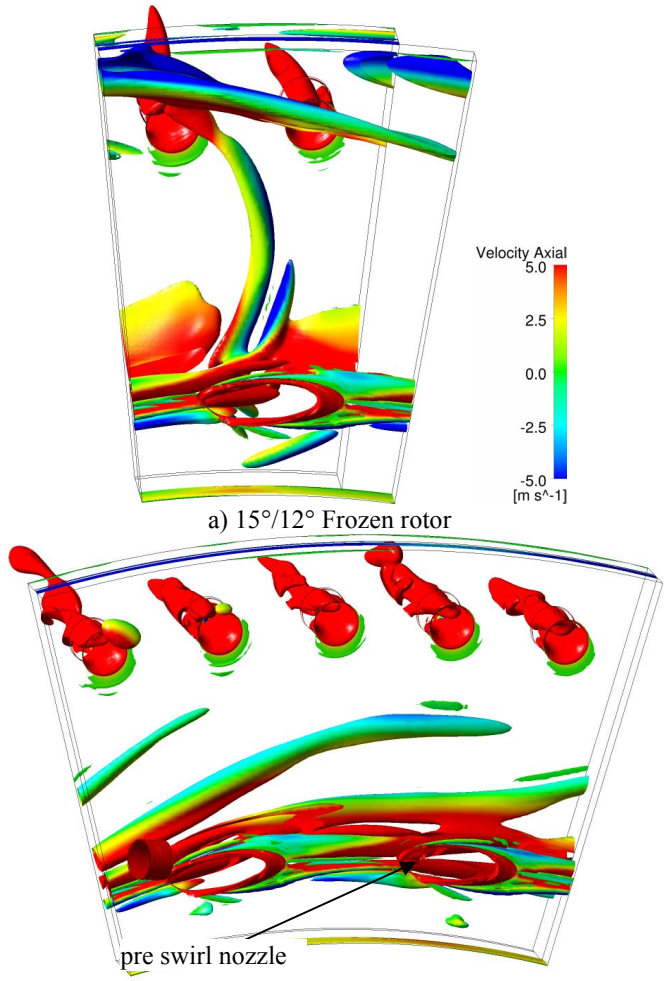

a) 15°/12° Frozen rotor
b) 30°/30° Transient

Figure 12: Vortical structures with Q = 4e+7 [1/s²] ($Re_\Phi = 1.2x10^6$, view through stator wall)

The vortex structures in the cavity can be seen in Figure 12. During the transient simulation the vortex structures are not stable they show depending on the relation between pre-swirl nozzle and receiver holes exit a slightly different shape. At each time step there is a different picture of high heat transfer zones

showing the overlapping of both mechanisms inducing high heat transfer. The full 30° sector model is better able to capture the interaction between two nozzle jets and their turbulence structures, than a 15°/12° sector with periodic boundary conditions. With the Stage interface the vorticity is "smoothed" in the circumferential direction at the interface resulting in radially-banded heat transfer contours. With the Frozen rotor interface the same streak found in the heat transfer coefficient can be seen in the vorticity. The frozen rotor simulation does not capture the transient flow effects due to the fixed position between pre-swirl nozzle and receiver holes, forcing the flow to take a different flow path.

Comparison with experimental values. Experimental values of the heat transfer coefficient are available along a radial line between two receiver holes. Especially at the pre-swirl nozzle radius the thermal impact on the rotor at a fixed point is oscillating, depending if the point crosses the pre-swirl jet or not. Therefore the experimental TLC measurement results are a circumferential time averaged observation of this oscillation.

The computed values of the heat transfer coefficient are taken from contour plots from the numerical simulations along a radial line mid-way between two receiver holes (Figure 13a), as well as using circumferentially averaged values of v_Φ and q_w (Figure 13b). Due to zones of high local heat transfer around the receiver holes in both, simulations and experiments (Lewis et al. [17]), a circumferential averaging is only meaningful at radii inward of the receiver holes.

Figure 13a) shows strong oscillations for the frozen rotor interface and the transient snapshots at the last time step. This is expected from the contour plots (Figure 11) but not helpful for comparison with the experimental values. Circumferential averaging at radii inward the receiver holes shows that the frozen rotor and transient results for the 15°/12° sector converge in the region outward of the pre-swirl nozzle radius (Figure 13b).

Comparison between the two transient averaged simulations with 15°/12° sectors and full 30° sector in Figure 13a) show small differences at pre-swirl nozzle radii. The peak value of the full 30° sector is smaller and the radial position of its peak better match the experimental values. This shift of the peak may result from the deflection of the pre-swirl jet outward of the nozzle radius r_p, perhaps due to secondary flow structures inward of r_p, which can be inferred (as blue vortices at $r < r_p$) in the contour plots of the transient simulations at the last time steps (Figure 11). These secondary flow structures are influenced by the scaling at the 15°/12° sector interface and may also be influenced by the sealing slot at the hub which is not modeled. The agreement for the heat transfer coefficient between the smaller 15°/12° sector and the full 30° sector is good enough to justify the smaller sector simplification for the domain.

The stage interface leads to lower heat transfer coefficients than the two transient simulations matching better to the measurement data, whereas it might be expected that the transient simulation should lead to the best numerical results for the approaches studied. The lower heat transfer coefficients with the stage interface are due to the circumferential averaging of the pre-swirl jet velocity at the interface and therewith the reduction of the impinging effects. As shown in Figure 10 the maximum circumferential velocity with the transient interface at the mid-surface is about 20 % higher than the averaged velocities with the stage interface.

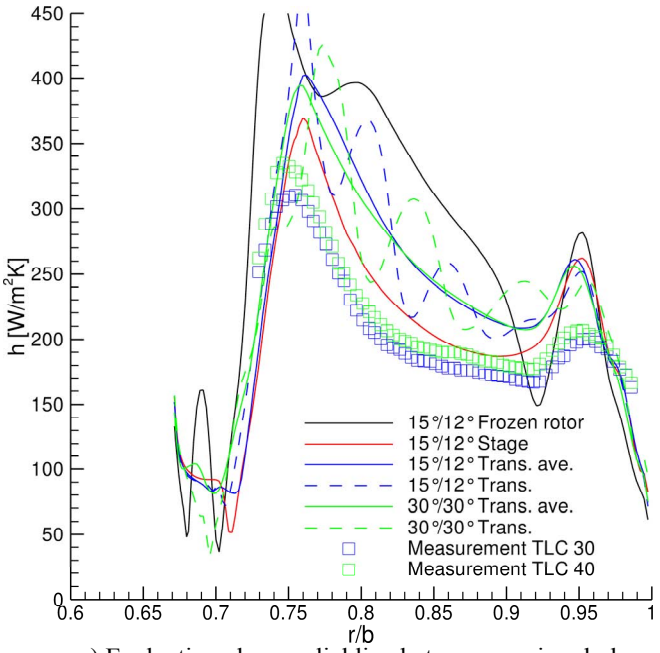

a) Evaluation along radial line between receiver holes

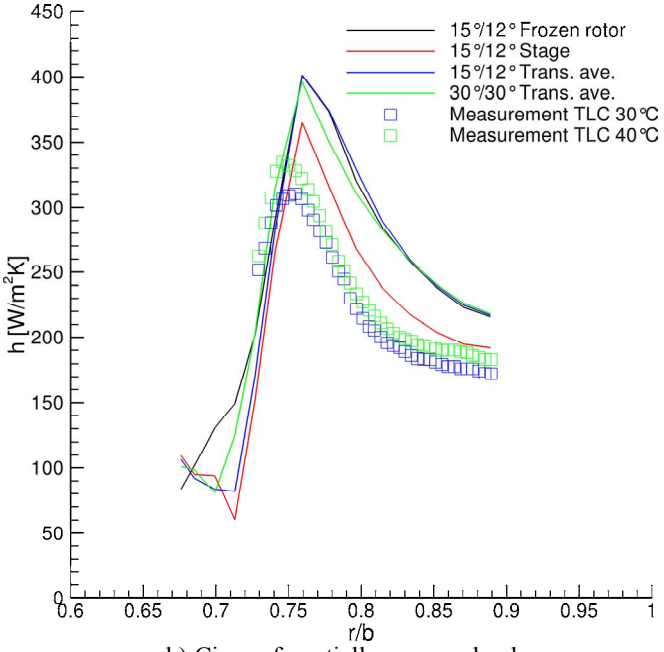

b) Circumferentially averaged values

Figure 13: Heat transfer coefficient distribution ($Re_\Phi = 1.2x10^6$)

This leads to heat transfer zones at the rotor with the transient interface where the local heat transfer is considerably higher than with the stage interface. This can be seen in Figure

14 where the wall heat flux from the numerical simulations for the stage and transient interface is evaluated along circumferential lines for two different radii. Even the transient averaged wall heat flux is higher than the one obtained with the stage interface.

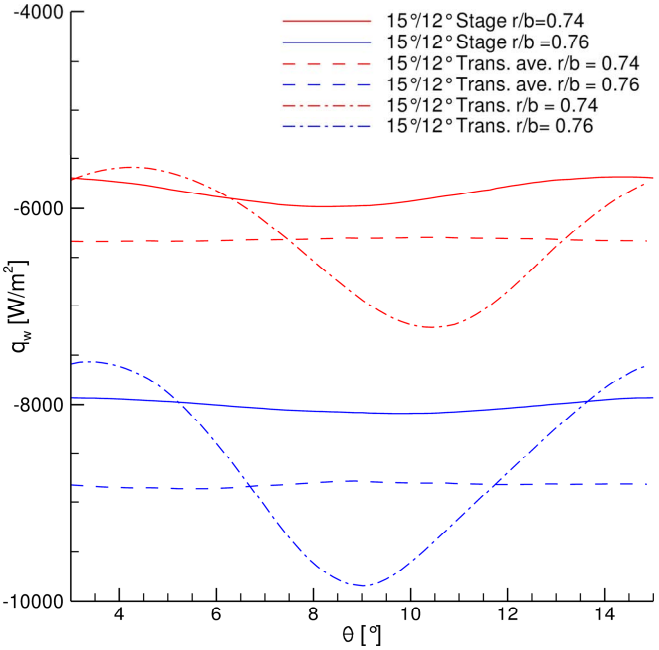

Figure 14: Circumferential evaluation of heat flux at the rotor for different interfaces at r/b = 0.74 and r/b = 0.76 ($Re_\Phi = 1.2x10^6$)

Comparing the circumferential averaged heat transfer results from the transient or frozen rotor simulation presented in this paper with the axisymmetric numerical model presented by Javiya et al. [12] (Fluent, SST k-ω turbulence model) show that the axisymmetric model show a stronger over prediction of the heat transfer around the pre-swirl nozzle radius. Compared with the 3D models using a circumferential inlet slot instead of a pre-swirl nozzle and using wall functions (Javiya et al. [12], Lewis et al. [18]) show that the simulations with the inlet slot predict usually a lower heat transfer around pre-swirl nozzle radius (lower impingement) but then over predict the heat transfer at r/b >0.8. 3D simulations with an inlet slot, a resolved near wall region and the k-ε turbulence model (Javiya et al. [12]) have shown a closer matching of the experimental values, but did not capture the specific heat transfer decay outward the pre-swirl nozzle radius. The 3D simulations with pre-swirl nozzle, wall functions and the k-ε turbulence model presented by Javiya et al. [12] show a closer matching of the experimental values. This indicates that the k-ε model predicts lower heat transfer values than the SST turbulence model even though the SST model is known to better approximate the near wall turbulence.

Variation with Re_Φ. To show the independency of the general heat transfer distribution from the rotational speed; simulations with all three interfaces were additionally carried out with a rotational Reynolds number $Re_\Phi = 0.8x10^6$. The comparison of heat transfer levels at a radial evaluation line between two receiver holes in Figure 15a) and the circumferentially averaged values for this cases in Figure 15b) show the same behavior between the three interfaces as at the higher rotational rotor speed. Only the level of the heat transfer coefficients differ from the results with $Re_\Phi = 1.2x10^6$. The reduced pre-swirl mass flow rate at lower Re_Φ required to achieve the same turbulent flow parameter λ_T leads to lower pre-swirl jet velocities and thus reduced impingement effects of the pre-swirl jet.

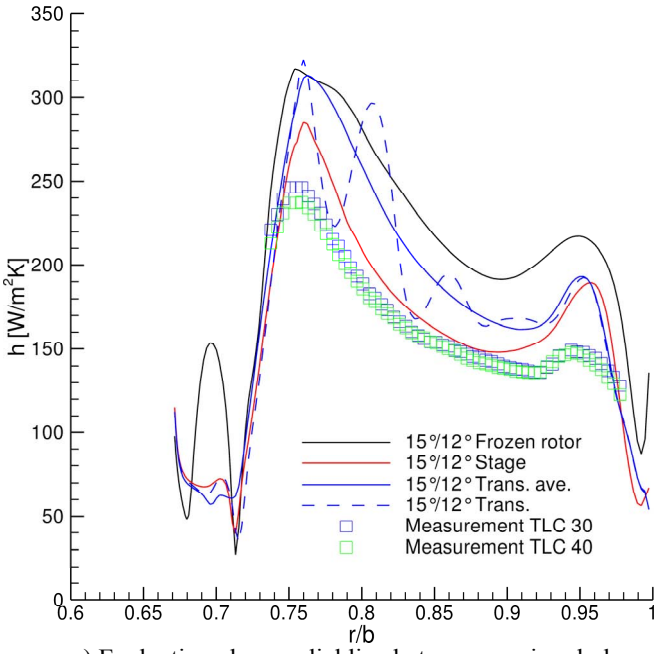

a) Evaluation along radial line between receiver holes

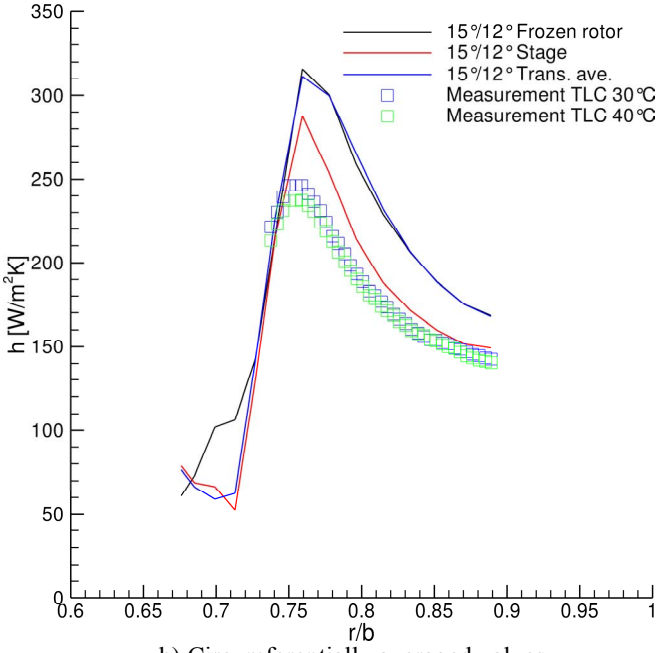

b) Circumferentially averaged values

Figure 15: Heat transfer coefficient distribution ($Re_\Phi = 0.8x10^6$)

CONCLUSIONS

For a low radius pre-swirl system numerical flow and heat transfer CFD simulations were carried out with a rotating and stationary model domain for pre-swirl ratios at nozzle radius β_p = 1.4 - 1.5. The influences of three different domain interface treatments (Frozen rotor, Stage and Transient) were compared amongst each other and with experimental results. As the experimental heat transfer coefficients at radii below the receiver holes radius provide circumferentially averaged information of transient heat transfer, numerical results were also circumferentially averaged.

The presented circumferentially averaged pressure distributions for the different interfaces show higher pressure differences between the interfaces around the pre-swirl nozzle radius r_p only. The pressure values converge outward the pre-swirl nozzle radius, which is also an inevitable consequence of the fixed outlet pressure boundary condition at the receiver holes. The circumferentially averaged velocity v_Φ shows only small variations between the different interfaces. The minimum and maximum values around the pre-swirl nozzle differ from the circumferentially averaged values about ± 25 % except for the stage interface where the velocity is smoothed at the interface.

Comparing contour plots of heat transfer coefficient h shows that the stage simulation and transient simulation with averaged values give the expected circumferential banded heat transfer, whereby the stage interface leads to lower heat transfer coefficient values due to the reduced impinging effect. The steady frozen rotor interfaces show a more complicated heat transfer pattern due to the fixed angular position between pre-swirl nozzle and receiver hole. Therefore if local heat transfer distributions are important the frozen rotor interface is not useful.

Evaluation of the heat transfer coefficient along a radial line between two receiver holes shows a strong oscillation of the heat transfer coefficient for the frozen rotor interface and the transient snapshot at the last time step. The circumferentially averaged heat transfer coefficient values show qualitative agreement with the experimental values. The frozen rotor and the transient simulation match together well but over predict the measured heat transfer. The stage interface leads to heat transfer results closest to experimental values but this is attributed to the smoothing of the pre-swirl jet at the stage interface, and therefore the reduction of the impingement effect.

The differences between the transient simulations for the full 30° domain and the simplified 15°/12° domain are small and justify the simplification to a smaller domain for circumferentially averaged values; nevertheless there are differences in local heat transfer distributions.

The different interface simulations were carried out for two different rotor speeds and these show qualitatively similar flow fields and heat transfer results between the three interfaces. Thus the information obtained concerning interface behavior could be transferred to other similar problems.

Even though the stage interface leads to the best agreement for averaged data with measured values this interface is less suitable for such kind of problem. A stage interface simulation where the interface crosses the pre-swirl jet is not able to predict the impinging effects of the pre-swirl jet and is therefore limited in a simulation with an over-swirled system. Only the transient simulation is able to describe fully the flow field and with this the impinging heat transfer situation. The circumferentially averaged values for the frozen rotor interface showed a good agreement with transient results. Therefore if only the circumferential averaged heat transfer values are important, the frozen rotor interface treatment leads to quite good and fast results compared to the time consuming transient simulations.

REFERENCES

[1] Celik I.B., Ghia U., Roache P.J., Freitas C.J., Coleman H. and Raad P.E., "Procedure for Estimation and Reporting of Uncertainty Due to Discretization in CFD Applications", Journal of Fluids Engineering, Vol.130:078001-1-078001-4, 2008

[2] Chen J.-X., Gan X., and Owen J.M., "Heat Transfer in an Air-Cooled Rotor Stator System", Journal of Turbomachinery, Vol. 118:444-451, 1996.

[3] Chew J.W., Ciampoli F., Hills N.J., and Scanlon T., "Pre-Swirled Cooling Air Delivery System Performance", ASME Paper GT2005-68323.

[4] Dittmann M., Dullenkopf K., and Wittig S., "Direct-Transfer Preswirl System: A One-Dimensional Modular Characterization of the Flow", Journal of Engineering for Gas Turbines and Power, Vol 127:383-388, April 2005.

[5] Dittmann M., Dullenkopf K., and Wittig S., "Discharge Coefficients of Rotating Short Orifices With Radiused and Chamfered Inlets", Journal of Engineering for Gas Turbines and Power, Vol 126: 803-808, October 2004.

[6] Dittmann M., Geis T., Schramm V., Kim S., and Wittig S., "Discharge Coefficients of a Preswirl System in Secondary Air Systems", Journal of Turbomachinery, Vol. 124:119-124, January 2002.

[7] Djaoui M., Dyment A., and Debuchy R., Heat transfer in a rotor-stator system with a radial inflow", European Journal of Mechanics - B/Fluids -20:371-398, 2001.

[8] Geis T., Dittmann M., and Dullenkopf K. "Cooling Air Temperature Reduction in a Direct Transfer Preswirl System", Journal of Engineering for Gas Turbines and Power, Vol 126:809-815, October 2004.

[9] Hunt J.C.R., Wray A.A., and Moin P. "Eddies, stream and convergence zones in turbulent flows", Center for Turbulence Research, CTR-S88, Stanford University, 1988

[10] Jarzombek K., Benra F.-K., Dohmen H.J., and Schneider O., "CFD Analysis of Flow in High-Radius Pre-Swirl Systems", ASME Paper GT2007-27404.

[11] Jarzombek K., Benra F.-K., Dohmen H.J., and Schneider O., "Flow Analysis in Gas Turbine Pre-Swirl Cooling Air Systems - Variation of Geometric Parameters", ASME Paper GT2006-90445.

[12] Javiya, U., Chew J., Hills N., Zhou L., Wilson M., and Lock G., “CFD Analysis of Flow and Heat Transfer in a Direct Transfer Pre-Swirl System, ASME Paper GT2010-22964.
[13] Kakade V.U., Lock G.D., Wilson M., Owen J.M., and Mayhew J.E., “Accurate heat transfer measurements using thermochromic liquid crystal. Part 2: Application to a rotating disc”, International Journal of Heat and Fluid Flow 30:950-959, 2009.
[14] Kakade V.U., Lock G.D., Wilson M., Owen J.M., and Mayhew J.E., “Effect of Radial Location of Nozzles on Heat Transfer in Pre-Swirl Cooling Systems”, ASME Paper GT2009-59090.
[15] Karabay H., Pilbrow R., Wilson M., and Owen J.M., “Performance of Pre-Swirl Rotating-Disc Systems”, Journal of Engineering for Gas Turbines and Power, Vol. 122:442-450, 2000.
[16] Karabay H., Wilson M., and Owen J.M., “Predictions of effect of swirl on flow and heat transfer in a rotating cavity”, International Journal of Heat and Fluid Flow 22:143-155, 2001.
[17] Lewis P., Wilson M., Lock G., and Owen J.M., “Physical Interpretation of Flow and Heat Transfer in Preswirl Systems”, Journal of Engineering for Gas Turbines and Power, Vol. 129:769-777, 2007.
[18] Lewis P., Wilson M., Lock G.D. and Owen J.M., “Effect of radial location of nozzles on performance of preswirl systems: a computational and theoretical study”, Proc. IMechE Vol 223 Part A:J.Power and Energy, 2009.
[19] Lock G.D., Wilson M., and Owen J.M., ”Influence of Fluid Dynamics on Heat Transfer in a Preswirl Rotating-Disk System”, Journal of Engineering for Gas Turbines and Power, Vol.127:791-797, 2005.
[20] Lock G.D., Yan Y., Newton P.J., Wilson M., and Owen J.M., ”Heat Transfer Measurements Using Liquid Crystals in a Preswirl Rotating-Disk System”, Journal of Engineering for Gas Turbines and Power, Vol.127:375-382, 2005.
[21] Meierhofer B., and Franklin C.J., “An Investigation of a preswirled cooling airflow to a turbine disc by measuring the air temperature in the rotating channels”, ASME Paper 81-GT-132, 1981.
[22] Newton P.J., Yan Y., Stevens N.E., Evatt S.T., Lock G.D., and Owen J.M., “Transient heat transfer measurements using thermochromic liquid crystal. Part 1: An improved technique”, International Journal of Heat and Fluid Flow 24:14-22, 2003.
[23] Owen J.M. and Rogers R.H., “Flow and Heat Transfer in Rotating-Disc Systems, Volume 2: Rotating Cavities”, John Wiley & Sons, New York Chichester Toronto Brisbane Singapore, 1995
[24] Pellé J. and Harmand S., “Heat transfer study in a discoidal system: The influence of rotation and space between disks”, International Journal of Heat and Mass Transfer 51: 3298-3308, 2008.
[25] Snowsill G.D. and Young C., “The Application of CFD to Underpin the Design of Gas Turbine Pre-swirl Systems”, ASME Paper GT2006-90443.
[26] Wilson M., Pilbrow R., and Owen J.M., “Flow and Heat Transfer in a Preswirl Rotor-Stator System”, Journal of Turbomachinery, Vol. 119:364-373, April 1997.
[27] Yan Y., Gord M.F., Lock G.D., Wilson M., and Owen J.M., “Fluid Dynamics of a Pre-Swirl Rotor-Stator System”, Journal of Turbomachinery, Vol. 125:641-647, 2003.